Comparing the bidomain and monodomain models in electro-cardiology through convergence analysis

Yves Bourgault, Charles Pierre

COMPARING THE BIDOMAIN AND MONODOMAIN MODELS IN ELECTRO-CARDIOLOGY THROUGH CONVERGENCE ANALYSIS

YVES BOURGAULT AND CHARLES PIERRE

Abstract. The monodomain and bidomain models are widely used in electro cardiology to simulate spreading of excitation potential waves in the myocardium. The bidomain model is quite popular for its physiological foundation and relevance whereas the monodomain model simply is a heuristic approximation of the previous one, lacking this physiological foundation but providing computational facilities. The purpose of the present article is to numerically compare these two models using a method of (numerical) convergence analysis. This method enables to reach two different objectives of first importance in biomedical engineering. Firstly it provides the discrepancy between the models at the continuous level (and not between the discretised equations only) by getting rid of the discretisation errors. Secondly, it allows to estimate the discretisation error so providing necessary grid resolution in order to run accurate enough simulation.
The comparison is held in terms of activation times, a quantity of major physiological importance. Two test cases are considered, both including enhanced cell membrane kinetic description, tissue anisotropy and realistic macroscopic tissue parameters. The first test case is based on an academic (a unit square) geometry. The second one involves a 2d cut of a segmented human heart. It has been built from 3D medical data of the two ventricles and incorporates anisotropy occurring from muscular fibre rotation around the ventricles.
Two conclusions are drawn from this study. In terms of activation time relative error, the discrepancy between the two models is quite small: of order 1% or even below. Moreover this error is smaller than the discretisation error resulting from commonly used mesh size in biomedical engineering.

1. Introduction

The bidomain model [29, 17, 1, 11, 30] is currently considered as the most accurate and physiologically founded description for the electrical cardiac behaviour and is widely used to simulate action potential spreading in the myocardium as well as electrocardiograms. Its mathematical formulation reads a system of two parabolic reaction diffusion equations, or equivalently one parabolic reaction diffusion equation coupled with one elliptic equation. This system is coupled with an ODE system describing cell membrane kinetics. The mathematical properties of the bidomain model are quite delicate to study. In [11] the bidomain model is studied under the form of a degenerate system of parabolic reaction diffusion

Date: February 9, 2011.
Key words and phrases. Electro-cardiology, bidomain and monodomain models, excitation process and activation time, reaction diffusion equations, numerical simulations, anisotropic diffusion.

equations. It has been shown in [3] that it can also be reformulated into one parabolic semi-linear PDE but including non locality in space. These structural properties (degeneracy in one hand, non locality on the other) bring numerical difficulties. One ill-conditioned linear system inversion is required per time step. Moreover cardiac action potential involving fast space and time potential variations, fine space and time grids must be considered. For these two reasons simulating the cardiac electrical activity with the bidomain model has a very high cost, and many efforts towards the reduction of this cost have been made, e.g. [9, 14, 8]. The monodomain model is a simplification of the bidomain model reading a single parabolic reaction diffusion equation (still coupled with the same ODE system modelling cell membrane). Although this simplification has no mathematical general justification, and although the monodomain model lacks physiological foundation, it is commonly used in electro-cardiology: firstly because it obviously lead to much lower computational efforts than the bidomain model (as analysed in [27]). The second reason motivating the interest for the monodomain model is that, as an approximation of the bidomain model, it may serve to improve numerical scheme efficiency for the bidomain model [16] or to build powerful preconditioners [15, 22]. The quality of the monodomain model approximation cam moreover be numerically optimised as developed in [20].

In comparison with the amount of papers dealing with the bidomain and the monodomain models, quite few studies measuring the discrepancy between these two models are available. In [10, 28], a precise approximation of the bidomain model, namely the adapted monodomain model (or modified monodomain), is stated and compared with the bidomain model. In [10], Colli-Franzone et al. compared the two models on an academic 3D test case, a small slab of cardiac tissue, including anisotropy (orthotropic or axysymmetric). Their comparison is based on activation time, recovery time and action potential duration measurements. They observed a strong qualitative agreement between the two models and a noticeable quantitative difference (5 to 10 % of relative error on the activation time e.g.). In [28], Potse et al. compared the two models on a complete 3D human hear. The discrepancy between the models is here reported to be small but not precisely measured (in terms of activation time, recovery time and epicardial potential measurements). Although a strong quantitative agreement for the epicardial potential depicted in the paper is clear, quantitative differences are again visible.

Meanwhile, Potse et al. in [28] brought to the fore a fundamental question: *"when comparing the bidomain and monodomain models, how to distinguish in the numerical results the amount of error due to the model choice from the amount of error caused by discretisation ?"* Precisely in [28], potential wave velocities have been measured for both models on two meshes of 0.1 and 0.2 mm resolution. On the finest grid the relative error on the longitudinal velocity predicted by the two models is of 2.5 %. The same longitudinal velocity predicted by the bidomain model on the two grids differ of 5.0 % (also of relative error). The error caused by discretisation then is twice larger than the measured discrepancy between the models. From the methodological point of view, no conclusion can be

drawn in such a situation concerning a quantification of the discrepancy between the bidomain and monodomain models.

This example also illustrate that even on very fine meshes the discretisation error might be as high as the model discrepancy. Appreciating this error is not easy. From the theoretical point of view, a posteriori error estimators for the quite complex bidomain model (involving enhanced reaction terms in practice) and especially designed for physiologically oriented criterion such as activation time or APD (action potential duration) have not be developed yet. From the numerical point of view, to the author knowledge very few studies intending to evaluate the discretisation errors through convergence analysis are available. Such a convergence study has been presented in [2] concerning the approximation of the bidomain model by *Discrete Duality Finite Volume* . Though the model setting was rather academical (involving in particular a very simplified cell membrane description), it illustrates that the convergence in terms of activation time is quite slow.

In this paper we propose a numerical methodology to evaluate the discrepancy between the bidomain and adapted monodomain models *at the continuous level*. Because of its particular physiological importance the comparison criterion is here set to the activation time, though the method used could also be applied to other criteria. The considered method is a convergence analysis for the two models allowing to evaluate the discretisation error and thus to get rid of it when evaluating the model discrepancy. The two following purposes of same practical importance in biomedical engineering are then addressed in this paper:

(1) measuring the discrepancy between the bidomain and monodomain models,
(2) evaluating the discretisation error and providing necessary grid resolution in order to obtain accurate simulations of cardiac spreading of excitation.

Two different test cases are considered in dimension 2, both involving complex ionic dynamics on the cell membrane and tissue anisotropy. A first test for an academic geometry on the unit square. A second test case on a 2D cut of a segmented human heart. For both test cases the Luo and Rudy class II model of cell membrane [19] (for mammalian ventricular cells) will be considered.

The paper is organised as follows. The bidomain and the adapted monodomain models are formulated in Sec. 2. In Sec. 3 is presented the methodology including the numerical implementation of the models and the two tests case presentation. The simulation results are given in Sec. 4. Results are discussed and conclusions are drawn in Sec. 5.

2. Models

The heart of a living organism is assumed to occupy a fixed domain Ω that is a bounded open subset of $\mathbb{R}^d$, $d = 2, 3$. At the macroscopic scale the cardiac tissue is considered as the superimposed of the intra-cellular *(i)* and extra-cellular *(e)* media. The *bidomain* and *adapted monodomain* models presented here describe the heart electrical activity at this scale.

For a derivation of the bidomain model from physiological considerations at the microscopic scale we refer to [29, 17, 1, 11, 30].

These two models involve two electrical potentials: the *intra-* and *extra-cellular potentials* $u_i,\ u_e :\ Q \mapsto \mathbb{R}$, where Q denotes the time-space cylinder $(0,T)\times\Omega$. Their difference is referred to as the *transmembrane potential*: $v := u_i - u_e\ :\ Q \mapsto \mathbb{R}$. The heart tissue has a fibrous organization into muscular fibres. This causes anisotropy for the electrical conductivity described by two conductivity tensors $\sigma_i(x)$ and $\sigma_e(x)$ at point $x \in \Omega$. Introducing the conductivities $g^l_{i,e},\ g^t_{i,e}$ longitudinal and transverse to the fibres, these tensors read:

$$\sigma_i(x) = \mathrm{Diag}(g^l_i, g^t_i), \quad \sigma_e(x) = \mathrm{Diag}(g^l_e, g^t_e), \tag{1}$$

in a moving system of coordinates whose principal direction is given by the fibre orientation at point x. The fibres are moreover assumed to be tangent to the heart boundary $\partial\Omega$.

In this paper, we consider the case of an isolated heart (the interaction with the surrounding tissues is neglected). This insulation assumption reads a zero flux boundary condition on u_i and u_e physically meaning that no current flows out of the heart. The fibres being tangent to $\partial\Omega$, this condition is equivalent with:

$$\nabla u_i \cdot \mathbf{n} = \nabla u_e \cdot \mathbf{n} = 0 \quad \text{on} \quad \partial\Omega, \tag{2}$$

$$\text{and so,} \qquad \nabla v \cdot \mathbf{n} = 0 \quad \text{on} \quad \partial\Omega. \tag{3}$$

2.1. **Bidomain model.** The bidomain model reads the three following equations, for $(t,x) \in Q$:

$$\begin{cases} \mathrm{div}((\sigma_i(x)+\sigma_e(x))\nabla u_e) = -\mathrm{div}(\sigma_i(x)\nabla v), \\ \chi\left(c\partial_t v + I_{ion}(v,\mathbf{w}) - I_{st}(t,x)\right) = \mathrm{div}(\sigma_i(x)\nabla(u_e+v)), \\ \partial_t \mathbf{w} = g(v,\mathbf{w}). \end{cases} \tag{4}$$

In equation 2, c denotes the membrane surface capacitance, χ is the rate of cell membrane surface per unit volume (homogenization parameter), $I_{st} :\ Q \mapsto \mathbb{R}$ is the stimulation current (source term). $I_{ion}(v,\mathbf{w})$ (reaction term) denotes the surface ionic current distribution on the membrane: its evolution is controlled by the gating variable $\mathbf{w}\ : Q \mapsto \mathbb{R}^N$ via the ODE system in line 3. The definitions of I_{ion} and of g are fixed by the chosen ionic model in 2.4.

Equations in (4) are closed by the boundary condition (2) and by an initial datum imposed on v and $\mathbf{w}$:

$$v(0,x) = v_0(x), \quad \mathbf{w}(0,x) = \mathbf{w}_0(x), \quad x \in \Omega. \tag{5}$$

Clearly, the bidomain model equations (4), (2) and (5) are invariant under the simultaneous change of $u_e,$, u_i into $ue + k$, $u_i + k$ for $k \in \mathbb{R}$: we therefore impose the normalization condition

$$\int_\Omega u_e(t,\cdot)dx = 0. \tag{6}$$

2.2. **Adapted monodomain model.** The adapted monodomain model is a simplification of the bidomain model where the transmembrane potential is simply defined by a parabolic reaction-diffusion equation, for $(t,x) \in Q$:

$$\begin{cases} \chi\left(c\partial_t v + I_{ion}(v,\mathbf{w}) - I_{st}(t,x)\right) = \operatorname{div}(\sigma_m(x)\nabla v), \\ \partial_t \mathbf{w} = g(v,\mathbf{w}), \end{cases} \tag{7}$$

with boundary condition (3) and initial condition (5). The conductivity tensor σ_m is defined as the harmonic mean between σ_i and σ_e,

$$\sigma_m^{-1}(x) := \sigma_i^{-1}(x) + \sigma_e^{-1}(x). \tag{8}$$

Again, since the fibres are tangent to the domain boundary, then $\sigma_m(x)\mathbf{n}$ and $\mathbf{n}$ have the same direction on $\partial\Omega$, so that (3) precisely is the classical homogeneous Neumann boundary condition on $\partial\Omega$ associated with the operator $\operatorname{div}(\sigma_m\nabla\cdot)$.

The potential $v : Q \mapsto \mathbb{R}$ being defined by equations (7) (3) (5), u_e can be recovered using the second equation in (4), this will not be discussed here.

2.3. **Comments.** In the adapted monodomain model framework, v is independent from u_e; whereas for the bidomain model, v and u_e are strongly coupled and in general none of these two quantities can be computed independently from the other one. This illustrates a complete difference of nature between these two models which we briefly discuss here.

In [3] it has been showed that the bidomain model can be reformulated in terms of v only as follows:

$$\chi\left(c\partial_t v + I_{ion}(v,\mathbf{w}) - I_{st}(t,x)\right) = \mathcal{A}v, \quad \partial_t \mathbf{w} = g(v,\mathbf{w}),$$

where $\mathcal{A}$ denotes the harmonic mean between the two elliptic operators $\operatorname{div}(\sigma_i\nabla\cdot)$ and $\operatorname{div}(\sigma_e\nabla\cdot)$. This operator is non-local in general, in the following sense: $\mathcal{A}u(x)$ is not determined by the values of u in a neighbourhood of the point x. Precisely, the definition of $\mathcal{A}u$ requires an elliptic problem inversion. The strong coupling between v and u_e precisely relies on this fact. However in some particular cases, namely in dimension 1 or in case of *equal anisotropy ratio* (i.e. if $\sigma_e(x) = k\ \sigma_i(x)$ for some constant $k \in \mathbb{R}$), one has the equality $\mathcal{A} = \operatorname{div}(\sigma_m\nabla\cdot)$ for the tensor σ_m in (8). In these cases, the two models coincide: they predict exactly the same transmembrane potential v.

These cases are exceptional. In general $\mathcal{A}$ is non local and the two models do not match. The adapted monodomain model thus is based on the heuristic approximation $\mathcal{A} \simeq \operatorname{div}(\sigma_m\nabla\cdot)$. Its motivation is to benefit from the numerical facilities provided by this approximation. On the contrary of the bidomain model, no physiological interpretation for (7) has to be sought.

We point out that the equal anisotropy ratio condition do not fit with the experimental data. The conductivities considered in this paper (introduced in the following subsection and given in Tab. 1) induce anisotropy ratios between the longitudinal and transverse directions of 9.0 and 2.0 for the intra and extra-cellular media respectively.

2.4. **Model settings.** In (4) and (7), the reaction terms I_{ion} and g are fixed by choosing an ionic model: such a model describes the ion transfer across the cell membrane due to the cell metabolism. The gating variable **w** being here aimed to characterise the state of the cell membrane. We consider in this paper the Luo and Rudy II model [19] that has been developed for mammalian ventricular cells.

Model parameters	**Value**	**Unit**
Cell membrane surface-to-volume ratio	$\chi \in [1000, 2000]$	$[\text{cm}^{-1}]$
Membrane surface capacitance	$c = 1.0$	$[\mu\ \text{F/cm}^2]$
Longitudinal intra-cellular conductivity	$g_i^l = 1.741$	[mS/cm]
Transverse intra-cellular conductivity	$g_i^t = 0.1934$	[mS/cm]
Longitudinal extra-cellular conductivity	$g_e^l = 3.906$	[mS/cm]
Transverse extra-cellular conductivity	$g_e^t = 1.970$	[mS/cm]

TABLE 1. Bidomain and adapted monodomain model parameters

All along this paper, the reference length and time scales are respectively set to the cm and ms. The macroscopic cardiac tissue parameters are displayed in Tab. 1. In this table F and S stand for the Faraday and the Siemens units.
Cardiac tissue conductivities are subject to strong individual variabilities [7, 26]: ranges for these values are available in the review paper [6]. In the present paper, conductivities are taken from [18]. The longitudinal to transverse conductivity ratio is of 9.0 for the intra-cellular media and of 2.0 for the extra-cellular media: thus clearly avoiding here the equal anisotropy ratio where bidomain and monodomain models do coincide, see Sec. 2.3. These conductivities induce an axial to transverse velocity ratio of 2.6. Setting χ to 1800 , axial and transverse velocities are of 0.5 and 0.19 m/s respectively, which data are in agreement with [26].
A wide range of values for the cell membrane surface to volume ratio χ also is available in the literature. In [25] the values of 3 300 and 6 600 cm^{-1} is reported for a human adult and neonatal heart respectively. A range of 2400 to 8400 cm^{-1} is provided in [6]. Beyond physiological questioning about valuing χ we only focus In this paper on the impact of its value for numerical computations. To measure this impact, a range of $\chi \in [1000, 2000]$ has been adopted here.

3. Methodology

3.1. **Numerical methods.** The following weak formulation of the bidomain model is considered, $\forall \psi \in H^1(\Omega)$:

(9)
$$\int_\Omega (\sigma_i + \sigma_e)\nabla u_e \cdot \nabla \psi dx + \int_\Omega \sigma_i \nabla v \cdot \nabla \psi dx = 0,$$

(10)
$$\chi c \partial_t \int_\Omega v\psi dx + \chi \int_\Omega (I_{ion}(v, \mathbf{w}) - I_{st}(x,t))\psi dx = \int_\Omega \sigma_i \nabla(u_e + v) \cdot \nabla \psi dx.$$

To this system is added the normalisation condition (6) to ensure uniqueness on u_e.

This formulation is discretised in time using an Euler semi-implicit scheme: implicit for the diffusion and explicit for the reaction. Spatial discretisation has been led using Control Volumes Finite Elements (CVFE, see eg [5]). One large linear system (symmetric and non-negative) has to be inverted at each time step. These inversions are the main numerical difficulty for the bidomain model: precise details on the implementation, and on the preconditioning of the bidomain model are available in [22].

The adapted monodomain model implementation is much simpler. We consider the classical weak formulation of the parabolic equation (7). It is discretised as for the bidomain model: using an Euler semi-implicit scheme in time and a CVFE discretisation in space.

Remark 1. *We eventually discuss the choice of the spatial discretisation. We numerically experimented that the result quality is highly sensitive to this choice. We compared 3 methods of order 2 (with respect to the mesh size) for the elliptic problem discretisation: P1 finite element, Discrete Duality Finite Volumes (DDFV, see eg* [12, 2] *as applied to the bidomain model) and Control Volumes Finite Elements (CVFE, see eg* [5]*). The CVFE method gave the best results and will be used here.*
For the CVFE method the nodes are located at the mesh vertices, allowing to associate to the numerical solution a P1 function on the mesh elements, which property will be useful in the next subsection

3.2. **Estimation of the errors.** One searches to measure the discrepancy between the bidomain and the adapted monodomain model at the continuous level. For this one needs to get rid of the errors caused by the discretisation. We proceed as follows:

- Firstly, we numerically study the convergence of the numerical schemes for both the bidomain and the adapted monodomain models, using series of successively refined meshes. An a posteriori error estimate then allows to evaluate the error induced by discretisation.
- Secondly, the error between the (discrete) bidomain and adapted monodomain models is computed on each mesh. Once this error becomes wider than the discretisation errors measured in step one, one can deduce the discrepancy between the (continuous) bidomain and adapted monodomain models.

Because of its particular physiological importance, we adopt an error criterion based on the activation time. Activation time $\phi : \Omega \mapsto \mathbb{R}$ is defined at each point x as the time $\phi(x)$ such that $v(\phi(x), x) = v_s$ for a threshold value v_s set here to $-20\ mV$. The value $\phi(x)$ tells us at what time the excitation wave reaches the point x. Activation time for test cases 1 and 2 are depicted on Figs. 2 and 5 respectively.

Let us denote by $\mathfrak{T}_n$ the series of meshes. We consider the numerical activation time ϕ_n computed relatively to $\mathfrak{T}_n$. We compare ϕ_{n-1} and ϕ_n by introducing the projection $\tilde{\phi}_{n-1}$ of ϕ_{n-1} on the finer level $\mathfrak{T}_n$. For this ϕ_{n-1} is considered as a P1 function (i.e. continuous piecewise affine) on the elements of $\mathfrak{T}_{n-1}$. The values of this function are computed on the vertices of $\mathfrak{T}_n$, which data allows to define the considered projection $\tilde{\phi}_{n-1}$ as a P1 function on the elements of $\mathfrak{T}_n$. The following relative error

in L^2 norm is computed, as well as the (logarithmic) convergence rate r_2^n with respect to the mesh number of vertices denoted D_n:

$$e_2^n := \|\tilde{\phi}_{n-1} - \phi_n\|_{L^2(\Omega)} \quad , \quad r_2^n := \frac{\log(e_2^{n-1}/e_2^n)}{\log(D_{n-1}/D_n)}. \tag{11}$$

An error estimator ε_2^n,

$$\frac{\|\phi_n - \phi_\infty\|_{L^2}}{\|\phi_\infty\|_{L^2}} \leq \varepsilon_2^n,$$

on the relative error between the discrete activation time mapping ϕ_n on $\mathfrak{T}_n$ and the activation time mappings ϕ_∞ for the continuous problem is defined as follows. The asymptotic behaviour of e_2^n is numerically analysed using r_2^n. Assuming that e_2^n has a geometrical behaviour with geometrical growth rate q, ie $e_2^n \simeq q e_2^{n-1}$, then we can derive the upper bound:

$$\begin{aligned}\|\phi_n - \phi_\infty\|_{L^2(\Omega)} &\leq \|\phi_n - \phi_{n+1}\|_{L^2(\Omega)} + \|\phi_{n+1} - \phi_{n+2}\|_{L^2(\Omega)} + \dots \\ &\leq \frac{q}{1-q}\|\phi_n - \phi_{n-1}\|_{L^2(\Omega)}.\end{aligned}$$

We thus will define

$$\varepsilon_2^n := \frac{q}{1-q}\frac{e_2^n}{\|\phi_M\|_{L^2(\Omega)}}, \tag{12}$$

with M the index of the finest mesh $\mathfrak{T}_M$.

We precise that saying that e_2^n has an asymptotic geometrical behaviour is equivalent with saying that r_2^n goes to a constant r, in which case q can be deduced from r.

We define the (relative) discrepancy between the bidomain and adapted monodomain models as:

$$\delta_2^n := \frac{\|\phi_n^b - \phi_n^m\|_{L^2(\Omega)}}{\|\phi_n^b\|_{L^2(\Omega)}}, \tag{13}$$

where b and m stands for bidomain and adapted monodomain respectively.

3.3. **Test cases.**

3.3.1. *Unit square.* The following academic test case is considered. The domain Ω is set to $[0,1]^2$, recalling that the cm is the reference length scale. A series of 6 meshes $(\mathfrak{T}_n)_{n=1,6}$ of this domain, from 177 to 160 385 vertices, has been considered. These 6 meshes are triangle regular meshes that have been generated using the *Matlab* mesher: the $(n+1)^{th}$ mesh is generated by cutting each triangle into 4 triangles. Thus, recalling that D_n denotes the number of vertices of $\mathfrak{T}_n$, we have $D_{n+1} = 4D_n$.
On this geometry the spreading of excitation potential waves is simulated as depicted on Fig. 2. Excitation is initiated by applying a centered stimulation during a short period of time, precisely: $I_{st}(x,t) = 52\ \mu A$ for $5 < t < 5.1$ and $|x - x_0| < 0.1$ (x_0 denoting the centre of Ω) and $I_{st}(x,t) = 0$ otherwise. Stimulation is applied at time $t = 5$ rather than $t = 0$ to ensure the ionic model to have reached its equilibrium rest state, which state might not be reached initially because of the large number of parameters in the Luo and Rudy II model and to possible rounding errors on these parameters.

The model parameters are set following the data in Tab. 1: three different values for χ will be considered: $\chi = 1000$, $\chi = 1500$ or $\chi = 2000$ cm^{-1}.
Initial condition (5) is taken as the rest state for the ionic model: $I_{ion}(v_0, \mathbf{w}_0) = 0 = g(v_0, \mathbf{w}_0)$. The domain Ω is assumed to be composed of a bundle of parallel horizontal muscular fibres, the following homogeneous tensors are defined:

$$\sigma_i(x) = \sigma_i := \mathrm{Diag}(g_i^l, g_i^t) \ , \quad \sigma_e(x) = \sigma_e := \mathrm{Diag}(g_e^l, g_e^t) \ . \tag{14}$$

3.3.2. *2D cut of a segmented heart.* We now consider a realistic 2D setting depicted on Fig. 1. The geometry has been obtained from the segmentation of a medical image of a human heart [23]: it represents a horizontal slice of the two ventricles with a resolution of 0.3 mm. The geometry has a surface of 27 cm^2.

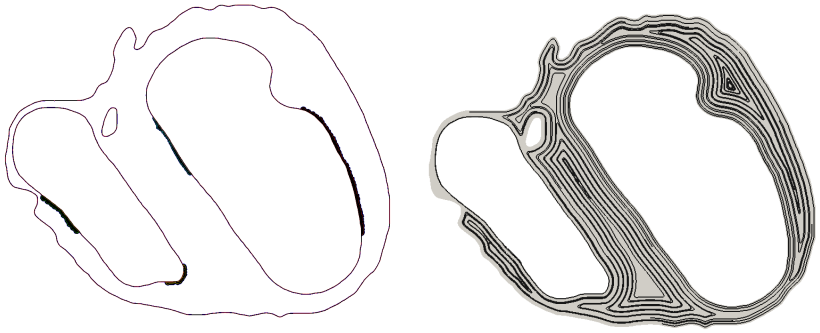

FIGURE 1. Test case 2 settings: stimulation sites location (above left) and fibrous structure of the tissue (above right).

Four meshes $(\mathfrak{T}_n)_{n=1,4}$ of this geometry have been built using the algorithm *Distmesh*[1] in [21]. These meshes precisely counting D_1 =117 285, D_2 =279 447, D_3 =551 484 and D_4 =1 110 270 vertices. Anisotropy is given from the fibrous organisation of the tissue following (1). A set of fibres rotating around the two ventricles and remaining tangent to the boundary has been built. Stimulation is initiated at 4 sites (two on each ventricle) on the endocardium. A stimulation current of 52 μA is applied during 0.1 ms at these locations at time 20 ms and 25 ms on the left ventricle and right ventricle respectively. The stimulation site locations as well as the delay of 5 ms between the stimulation of the left and of the right ventricles is aimed to mimic experimental measurements on a perfused heart in [13]. Stimulation is initiated at time t=20 ms rather than $t = 0$ for the same reason as in the Unit Square test case.

The model parameters are set following the data in Tab. 1, χ is here set to $\chi = 1500$ cm^{-1}.

4. RESULTS

4.1. **Unit square.** The spreading of transmembrane potential wave v (after centered stimulation at time $t = 5$ ms) is depicted on Fig. 2 for

[1]DistMesh: *"a simple mesh generator in Matlab"*, http://www-math.mit.edu/ persson/mesh/

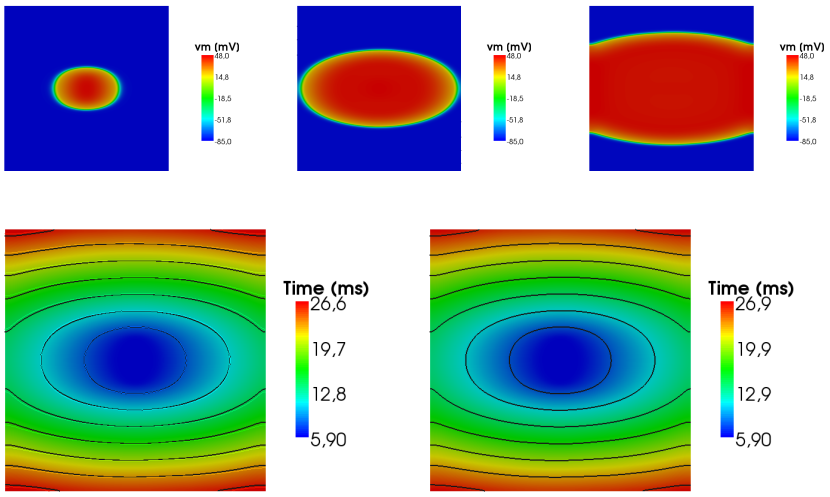

Bidomain Monodomain

FIGURE 2. Above: spreading of transmembrane potential wave after stimulation (for the monodomain model, $\chi = 1500$). Potential maps are represented 3, 8 and 12 ms after the stimulation. Below: comparison of the activation time mappings predicted by the bidomain (left) and adapted monodomain (right) models, on the finest mesh and also for $\chi = 1500$ cm^{-1}.

the adapted monodomain model and for $\chi = 1500$ cm^{-1} on the finest mesh. On Fig. 2 are also depicted the resulting activation time mappings for the bidomain and adapted monodomain models. As a first observation, activation time predicted by both models are in qualitative agreement, isolines displaying the same expected elliptical shape. A first and simple quantitative comparison criterion on the propagation velocities also shows the concordance between the two model predictions: the total time for the depolarisation wave to recover the whole domain is of 21.6 and 21.9 ms for the bidomain and monodomain models. Although the bidomain model appears to be slightly faster, the relative error between these figures is of 1.4 %. This estimation can be reinforced by comparing the relative error between the L^2 norm of the activation time mappings:

$$e_0 = \frac{\|\phi_{mono}\|_{L^2} - \|\phi_{bid}\|_{L^2}}{\|\phi_{bid}\|_{L^2}}. \tag{15}$$

Computed on the finest mesh, we get $e_0 = 0.85\ 10^{-2}$, $0.97\ 10^{-2}$ and $1.07\ 10^{-2}$ for $\chi = 1000$, 1500 and 2000 respectively.

Numerical results on the convergence e_2^n and convergence rate r_2^n of the activation time mappings in L^2 norm are displayed in Tab. 2 and Tab. 3 for the bidomain and adapted monodomain models respectively. For both models the convergence of the activation time mapping is clearly observed; it is moreover reasonable to assume an order -1 convergence with respect to the mesh number of vertices D_n. This order -1 convergence justifies the definition of the error estimator ε_2^n in equation (12) taking

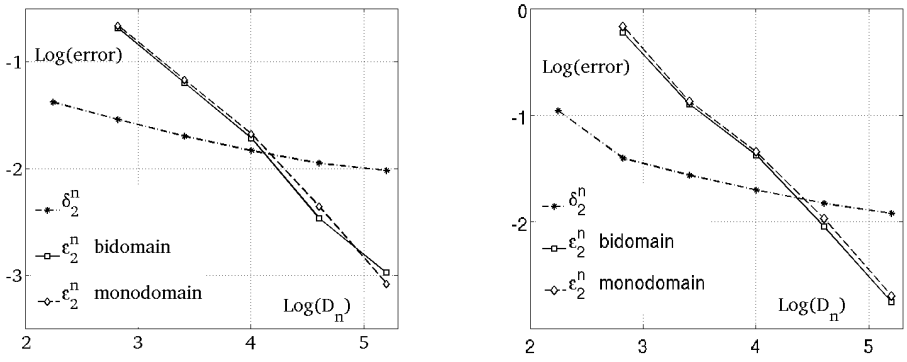

$\chi = 1000$ cm^{-1} $\chi = 2000$ cm^{-1}

FIGURE 3. Comparison of the discretisation error ε_2^n (defined in (12)) between the continuous and discrete solution and of the relative discrepancy δ_2^n (defined in (13)) between the bidomain and monodomain models activation times in L^2 norm. The comparison is depicted simultaneously for the bidomain and monodomain models and for two values of χ.

$q = 1/4$, since D_n is here multiplied by 4 each time n is incremented of 1.

Results on the error estimator ε_2^n are given in Tab. 4 for both models. They also are displayed on Fig. 3 for the two values of $\chi = 1000$ and $\chi = 2000$. Three immediate conclusions can be drawn from these figures. Firstly the discretisation errors are quite similar for the bidomain and the monodomain models. Secondly the discretisation error increases with χ. Thirdly, obtaining a precise approximation using physiological values of the parameter χ necessitates to consider very fine meshes. These three points will be discussed deeper on in the conclusion section 5.

The relative discrepancy δ_2^n between the (discrete) bidomain and adapted monodomain models is quantified in Tab. 5. Numerical results in Tabs. 4 and 5 are summarised on Fig. 3 for $\chi = 1000$ and $\chi = 2000$. These results clearly indicate that the discretisation error becomes smaller than the discrepancy between the two models on the two finest meshes. More precisely the discrepancy between the two models is larger than the discretisation error with roughly a factor 10 on the finest mesh. Thus the discrepancy between the bidomain and the adapted monodomain models on this test case appears to be smaller than 1%.

This estimation can be refined by examining more carefully the data in Tab. 5. The sequence δ_2^n decreases towards its limit for the three considered values of χ, which limit we can try to extrapolate from the data. On Fig. 4 is depicted δ_2^n as a function of $1/D_n$ (D_n still denoting the number of vertices of the mesh $\mathfrak{T}_n$) in decimal logarithmic scale. For all the three considered values of χ the plots display an almost linear behaviour. The slopes have been evaluated using a least square approximation taking into account the 5 last data points only (i.e. skipping δ_2^1). The results respectively are of 2.98, 3.10 and 3.20 for $\chi = 1000$, 1500 and 2000. This means a convergence of order -0.33, -0.32 and -0.31 respectively of δ_2^n

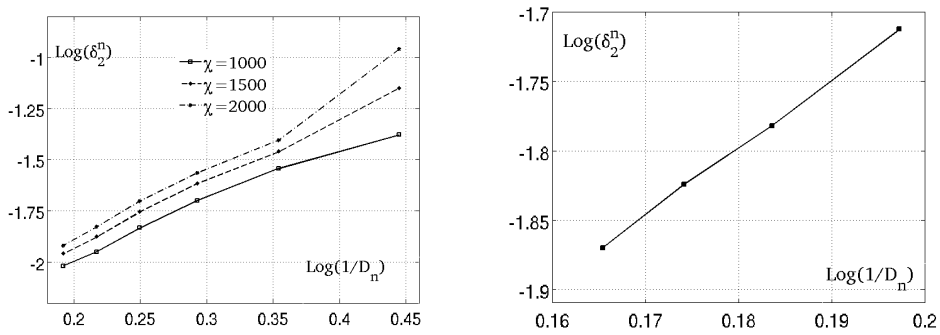

FIGURE 4. Extrapolation of the limit for δ_2^n as $n \to +\infty$. The discrepancy between the two models is depicted as a function of $1/D_n$ in decimal logarithmic scale. Left: unit square test case, for the three considered values of χ. Right: 2D cut of a segmented heart test case.

with respect to D_n. From this we can conclude to a convergence of order -1/3 of δ_2^n with respect to the mesh number of vertices. The limit of δ_2^n is then extrapolated by considering the intersection of this least square best linear approximation of the 5 last data points with the y axis. The extrapolated limits for δ_2^n are of 0.26 %, 0.29 % and 0.30 % for $\chi = 1000$, 1500 and 2000 respectively.

We eventually point out that although these extrapolated limit values are 2 to 3 times larger than the estimated discretisation errors in Tab 4 on the finest mesh, our numerical results remain too rough to provide a precise approximation such as 0.3 %. We can however conclude that on this test case, for the three considered values of χ, the relative discrepancy in L^2 norm between the activation time mapping predicted by the bidomain and the adapted monodomain models is 2 to 3 times smaller than 1 %.

4.2. **2D cut of a segmented heart.** The spreading of transmembrane potential wave v across the 2D segmented heart geometry is depicted on Fig. 5 using the bidomain model (and for $\chi = 1500$ cm^{-1}, which value is fixed in this section). The activation time mappings simulated using the bidomain and adapted monodomain models are displayed on the same Fig. 5. As for the first test case, these activation times are in good qualitative agreement. The total amount of time for the depolarisation wave to recover the whole domain is of 77.48 and 79.34 ms for the bidomain and monodomain models. The bidomain model again appears as being slightly faster, the relative error between these two times is of 2.4 %. Computing the relative error between the L^2 norms of the activation time mappings e_0 defined in (15) here gives $e_0 = 1.18\ 10^{-2}$.

The numerical results on the convergence are given in Tab. 6. We here observe a convergence block between the third and the fourth mesh. Although the L^2 distance $\|\tilde{\phi}_n - \phi_{n-1}\|_{L^2}$ for $n = 2$, 3 normally decreases (with a convergence rate $r_2^3 \simeq -0.6$ that could be in good agreement with a -1 order of convergence with respect to D_n as observed for the previous test case), this distance stops decreasing between meshes 3 and 4. This convergence block moreover very similarly occurs for the bidomain and

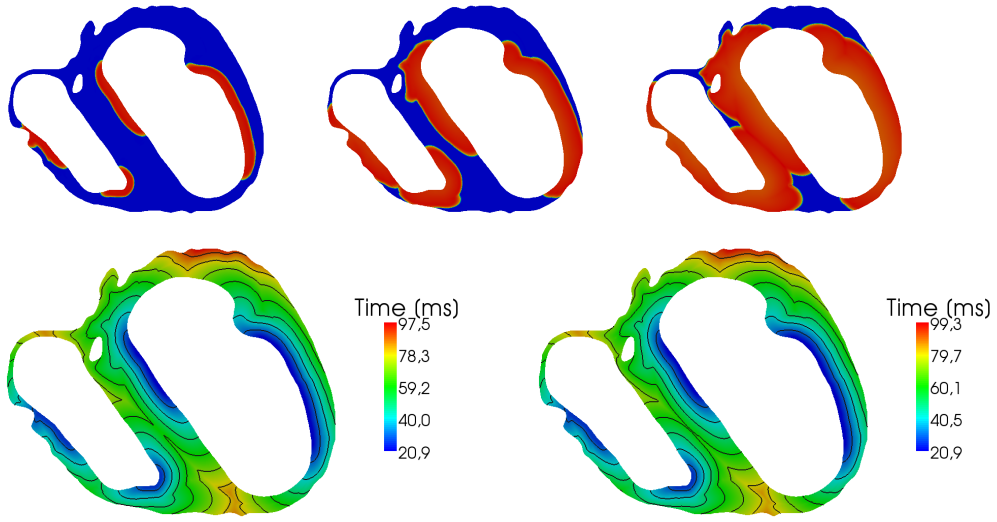

Bidomain Monodomain

FIGURE 5. Above: spreading of transmembrane potential wave across the segmented heart geometry, simulated using the bidomain model on the finest mesh, $\chi = 1500$ cm^{-1}. Potential maps are represented 16, 32 and 48 ms after the stimulation. Below: comparison of the activation time mappings predicted by the bidomain (left) and adapted monodomain (right) models, also on the finest mesh. Isolines (in black) are separated by 10 ms. Stimulation is initiated at time $t = 20$ ms.

adapted monodomain models. Several assumptions can be advanced to explain this phenomenon, that all rely on the quite complex setting of this test case. The *numerical geometry* (the union of all triangles of the mesh $\mathfrak{T}_n$) is not fixed. Practically, the inputs for the mesh construction using the software *Distmesh* are the mesh size and a level set function. This level set function itself is numerically defined on the underlying segmentation grid. Because of the relative complexity of the segmented domain, $\mathfrak{T}_n$ and $\mathfrak{T}_{n+1}$ may not exactly recover the same region, so inducing boundary errors for the projection $\tilde{\phi}_n$ of ϕ_n on $\mathfrak{T}_{n+1}$. The anisotropy tensors are not analytically defined and so do not converge to some limit tensor: the anisotropy has been defined on the image segmentation grid and simply projected on each meshes. This also is a plausible sourde of error inducing the convergence block.

Despite this convergence block, the discretisation error estimator ε_2^n however has been computed as in the previous test case (that is assuming a -1 order convergence with respect to the mesh number of vertices), the results also are given in Tab 6. From these figures, it seems acceptable to bound the relative discretisation error on the finest meshes to a few percent: 3 to 4 %.

This range of discretisation error has to be put into perspective with the first test case. The domain surface here is of 27 cm^2 and the finest mesh approximately counts 40 000 vertices per cm^2, and thus has the same resolution as mesh 5 of the unit square. The discretisation error was

for this mesh however 6 to 8 times smaller than presently. The complex setting of this test case then induces a supplementary and significant amount of discretisation error.

The relative discrepancy δ_2^n between the bidomain and adapted monodomain models itself do present a much finer behaviour that is depicted on Fig. 4, data are precisely reported in Tab. 7. In decimal logarithmic scale, δ_2^n displays a linear dependence with $1/D_n$, with slope 4.9 (using a least square best approximation of the data with a linear mapping). Thus δ_2^n seems to converge towards its limit with an order -1/5 convergence with respect to the mesh number of vertices. Here again we observe a slow down in the convergence as compared to the first test case where the convergence (already quite slow) had been evaluated to be of order $-1/3$ with D_n. Extrapolating the limit from this data provides us a discrepancy between the continuous bidomain and adapted monodomain models of 0.2 %.

Because of the convergence block previously discussed, and to the amount of discretisation error evaluated to 3 to 4 %, it is not reasonable to raise such a conclusion. From the quality of the result on δ_2^n, we however conclude to a discrepancy of order 1 % or even below 1 % between the activation time mappings of the continuous bidomain and adapted monodomain models.

5. Discussion

This paper was aimed to present a precise and numerically documented comparison of the bidomain and adapted monodomain models for the simulation of cardiac electro-physiology. The models definition, their numerical implementation and the general methodology for their comparison has been clearly stated. The comparison methodology relies on two points: the definition of a physiologically relevant comparison criterion (based on activation time comparison) and a numerical convergence analysis of the two models to get rid of discretisation errors. Comparison has been led on two test cases both involving complex ionic dynamics and realistic macroscopic tissue parameter settings: the first one for an academic unit square geometry and the second one for a complex 2D cut of segmented human ventricles.

Two main conclusions are drawn by analysing these two test case results,

(1) the amount of error caused by discretisation for commonly used grid resolutions is quite high,
(2) the discrepancy between the two model predictions is very small, of order 1 % or even below 1 % of relative error in L^2 norm.

5.1. **Discretisation error.** The (relative) discretisation error on the activation time has been evaluated on the two test cases. For both test cases, this amount of error has been quantified to be quite large even for *fine grids* (i.e. fine when compared to the mesh size commonly used in biomedical engineering). This error moreover increases when going towards complex settings. On the contrary, skipping from the bidomain to the monodomain model has no real influence on this error. To the

author appreciation, once the ionic model set, the main factor of discretisation error is the value of the parameter χ. The influence of χ on the discretisation error has been evaluated for the unit square test case. As expected, the highest χ, the largest the discretisation error. Indeed, for both the bidomain and the monodomain models, χ could be rescaled to the value of 1 by changing the space variable x into $x\sqrt{\chi}$. Therefore the mesh number of vertices has to be proportional to $\chi^{d/2}$ (with d the space dimension). More phenomenologically, the greatest χ the sharpest the wave fronts: thus more points are needed to obtain a good approximation inside the wave front location. The number of points needed transversally to the wave front then is proportional to $\sqrt{\chi}$.
The physiological range of values for χ (from 2400 to 8400 cm^{-1} in [6]) then imply very important computational efforts. Numerical simulations based on the bidomain or the monodomain models commonly depreciate this value (from 1000 to 2000 in this paper, χ =1000 in [10, 28], $\chi = 500$ in [24, 4], e.g.). As a simple illustration: to predict activation times with a tolerance relative error of 5 % using the (physiologically still under estimated) value $\chi = 2000$ cm^{-1} necessitates to require a mesh resolution of 0.1 mm on the unit square test case or even less for more complex simulation. This would mean more than 1 million of points per cm^3 in dimension 3. Asking for a 1 % relative error would increase this figure to 8 million points per cm^3 (0.05 mm resolution grid). Although these estimations are quite rough, context depending and could be decreased using more accurate numerical methods (increasing the order e.g.), *we conclude that running accurate simulations of cardiac electrical activity remains challenging in this context for physiological values of the parameter χ.*

5.2. **Model comparison.** For the two test cases the discrepancy has been evaluated to be of order 1 % in terms of L^2 activation time relative error.
The first test case involved a simple anisotropy type for the tissue and a simple central excitation that resulted into basic patterns of excitation: elliptical isolines for the activation time. The discrepancy in this case has been evaluated to be even smaller than 1 % and was bounded above by 1/2 or 1/3 % (uncertainties remaining due to numerical noise).
The second test case involved a much more sophisticated setting in terms of geometry, anisotropy and stimulation settings inducing enhanced patterns of excitation. Although the discrepancy analysis was made harder in this case, we concluded to *an order 1 % or even below* of relative error between the two models.

The following two points are interesting to notice. Firstly the discrepancy was measured for three values of χ in the first test case: 1000, 1500 and 2000 cm^{-1}. In first approximation the influence of χ is not visible. Secondly the discretisation imply an over-estimation of the model discrepancy: in Tabs. 5 and 7, δ_2^n decreases with the mesh size.

Although we obtained a comparable order of discrepancy between the models for two quite different test cases, our reported order of 1 % of error cannot be generalised and its dependence with the model parameters still need to be evaluated. As already mentioned χ has no important

influence on the model discrepancy. However the conductivities might have a great impact since in case of equal anisotropy the discrepancy is of zero. Considering the following ratio ρ:

$$\rho = \frac{g_i^l/g_i^t}{g_e^l/g_e^t},$$

equal to 1 in case of equal anisotropy ratio and satisfying $\rho > 1$ in physiological settings. The model discrepancy is expected to grow up with ρ.

The only reported bidomain and monodomain discrepancy in terms of activation time comparison available in the literature (and also computed using L^2 norms) is available in [10]. In this paper Colli-Franzone et al. measured this discrepancy on a 3D slab of tissue either with axisymmetric or orthotropic anisotropy. They measured a significantly higher discrepancy than we did: 6.3 % and 11.3 % for the two different anisotropic settings respectively. Although they considered a different ionic model (Luo and Rudy type I model) and a different value of χ (1000 cm^{-1}) we think that the observed difference rather lies in the two following points. Firstly the conductivities in [10] imply a value of $\rho = 7.1$ whereas $\rho = 4.5$ here: we then are further from the equal anisotropy ratio in this paper. Secondly the mesh size in [10] is of 0.1 mm. The discretisation error on such a fine grid might remain high in a complex 3D anisotropic setting leading to an over estimation of the model discrepancy.

5.3. **Conclusion.** The discrepancy between the (continuous) bidomain and adapted monodomain models has been evaluated to be of order 1 % in terms of relative error on the activation time. This is quite small: such a range of error is negligible for a field (biological sciences) where the tolerance on the data errors is much larger. Meanwhile the amount of error induced by the discretisation shall be even higher than the model discrepancy for commonly used mesh resolution in biomedical engineering. Therefore, to the authors feeling, the monodomain model should be preferred to the bidomain model to simulate patterns of excitation in the cardiac tissue taking advantage of its lightest implementation and computational cost.

References

[1] L. Ambrosio, P. Colli-Franzone, and G. Savaré. On the asymptotic behaviour of anisotropic energies arising in the cardiac bidomain model. *Interfaces Free Bound.*, 2(3):213–266, 2000.

[2] B. Andreianov, M. Bendahmane, K. H.. Karlsen, and C. Pierre. Convergence of DDFV schemes for the bidomain cardiac model. *HAL Preprint*, 2010.

[3] Y. Bourgault, Y. Coudière, and C. Pierre. Existence and uniqueness of the solution for the bidomain model used in cardiac electrophysiology. *Nonlinear Analysis: Real World Applications*, 10(1):458–482, 2009.

[4] M.L. Buist and A.J. Pullan. The effect of torso impedance on epicardial and body surface potentials: a modeling study. *IEEE Trans. Biomed. Eng.*, 50(7):816–824, 2003.

[5] Z. Cai, J. Mandel, and S. McCormick. The finite volume element method for diffusion equations on general triangulations. *SIAM J. Numer. Anal.*, 28:392–403, 1991.

[6] R.H. Clayton, O. Bernus, E.M. Cherry, H. Dierckx, F.H. Fenton, L. Mirabella, A.V. Panfilov, F.B. Sachse, G. Seemann, and H. Zhang. Models of cardiac tissue electrophysiology: Progress, challenges and open questions. *Progress in Biophysics and Molecular Biologyÿ*, 104:22–48, 2011.

[7] L. Clerc. Directional differences of impulse spread in trabecular muscle from mammalian heart. *J. Physio.*, 255(2):335–346, 1976.

[8] P. Colli Franzone, P. Deuflhard, B. Erdmann, J. Lang, and L. F. Pavarino. Adaptivity in space and time for reaction-diffusion systems in electrocardiology. *SIAM J. Sci. Comput.*, 28(3):942–962 (electronic), 2006.

[9] P. Colli Franzone and L.F. Pavarino. A parallel solver for reaction-diffusion systems in computational electrocardiology. *Math. Models Methods Appl. Sci.*, 14(6):883–911, 2004.

[10] P. Colli-Franzone, L.F. Pavarino, and B. Taccardi. Simulating patterns of excitation, repolarization and action potential duration with cardiac Bidomain and Monodomain models. *Math. Biosci.*, 197(1):35–66, 2005.

[11] P. Colli-Franzone and G. Savaré. Degenerate evolution systems modeling the cardiac electric field at micro- and macroscopic level. *Evolution equations, semigroups and functional analysis*, 2002.

[12] Y. Coudiere, C. Pierre, O. Rousseau, and R. Turpault. 2D/3D DDFV scheme for anisotropic- heterogeneous elliptic equations, application to electrograms simulation from medical data. *Int. J. Finite Volumes*, 2009.

[13] D. Durrer, RT. Van Dam, GE. Freud, Janse MJ., Meijler FL., and ArzBaecher RC. Total excitation of the isolated human heart. *Circulation*, 41:899–912, 1970.

[14] M. Ethier and Y. Bourgault. Semi-implicit time discretization schemes for the bidomain model. *SIAM Journal of Numerical Analysis*, 46(5):2443–2468, 2008.

[15] L. Gerardo-Giorda, L. Mirabella, F. Nobile, M. Perego, and A. Veneziani. A model-based block-triangular preconditioner for the bidomain system in electrocardiology. *J. Comput. Phys.*, 228(10):3625–3639, 2009.

[16] L. Gerardo-Giorda, M. Perego, and A. Veneziani. Optimized schwarz coupling of bidomain and monodomain models in electrocardiology. *M2AN*, 2010.

[17] W. Krassowska and J.C. Neu. Homogenization of syncytial tissues. *CRC Crit. Rev. Biomed. Eng.*, 21(2):137–199, 1993.

[18] P. Le Guyader, F. Trelles, and P. Savard. Extracellular measurement of anisotropic bidomain myocardial conductivities. I. theoretical analysis. *Annals Biomed. Eng.*, 29(10):862–877, 2001.

[19] C.H. Luo and Y. Rudy. A Dynamic Model of the Cardiac Ventricular Action Potential I. Simulations of Ionic Currents and Concentration Changes. *Circ. Res.*, 74:1071–1096, 1994.

[20] B.F. Nielsen, T.S. Ruud, G.T. Lines, and A. Tveito. Optimal monodomain approximations of the bidomain equations. *Applied Mathematics and Computation*, 184:276–290, 2007.

[21] P. O. Persson and G. Strang. A simple mesh generator in matlab. *SIAM Review*, 46(2):329–345, 2004.

[22] C. Pierre. Preconditioning the coupled heart and torso bidomain model with an almost linear complexity. *HAL Preprint*, 2010.

[23] O. Rousseau. Geometrical modeling of the heart. *PHD Thesis, University of Ottawa*, 2010.

[24] N.P. Smith, M.L. Buist, and A.J. Pullan. Altered t wave dynamics in contracting cardiac model. *J. Cardiovascular Electrophysio.*, 14:5203–5209, 2003.

[25] M. S. Spach, J. F. Heidlage, P. C. Dolber, and R.C. Barr. Electrophysiological Effects of Remodeling Cardiac Gap Junctions and Cell Size . *Circ. Res.*, 86(3):302–311, 2000.

[26] MS. Spach, JF. Heidlage, PC. Dolber, and RC. Barr. Extracellular Discontinuities in Cardiac Muscle Evidence for Capillary Effects on the Action Potential Foot . *Circ. Res.*, 83:1144–1164, 1998.

[27] J. Sundnes, B.F. Nielsen, K.A. Mardal, X. Cai, G.T. Lines, and A. Tveito. On the computational complexity of the bidomain and the monodomain models of electrophysiology. *Annals of Biomedical Engineering*, 34:1088–1097, 2006.

[28] MC. Trudel, B. Dube, M. Potse, RM. Gulrajani, and LJ. Leon. Simulation of qrst integral maps with a membrane-based computer heart model employing parallel processing. *IEEE Trans. Biomed. Eng.*, 51(8):1319– 1329, 2004.
[29] L. Tung. A bidomain model for describing ischemic myocardial D-D properties. *Ph.D. thesis, M.I.T..*, 1978.
[30] M. Veneroni. Reaction-diffusion systems for the microscopic cellular model of the cardiac electric field. *Math. Methods Appl. Sci.*, 29(14):1631–1661, 2006.

Appendix A. Tables

n	D_n	$\chi = 1000$		$\chi = 1500$		$\chi = 2000$	
		e_2^n	r_2^n	e_2^n	r_2^n	e_2^n	r_2^n
1	177						
2	665	9.20		17.7		32.4	
3	2 577	2.82	-0.87	4.79	-0.96	6.91	-1.14
4	10 142	0.851	-0.88	1.53	-0.83	2.29	-0.81
5	40 257	0.151	-1.25	0.300	-1.18	0.490	-1.12
6	160 385	$4.66\ 10^{-2}$	-0.85	$6.89\ 10^{-2}$	-1.06	$9.63\ 10^{-2}$	-1.18

Table 2. Unit square. Bidomain model: convergence of the activation time ϕ_n. The error indicator e_2^n and convergence rate r_2^n being defined in (11).

n	D_n	$\chi = 1000$		$\chi = 1500$		$\chi = 2000$	
		e_2^n	r_2^n	e_2^n	r_2^n	e_2^n	r_2^n
1	177						
2	665	9.79		19.6		37.7	
3	2 577	3.04	-0.86	5.15	-0.99	7.44	-1.20
4	10 142	0.949	-0.85	1.68	-0.82	2.49	-0.80
5	40 257	0.198	-1.14	0.314	-1.09	0.590	-1.05
6	160 385	3.7310^{-2}	-1.21	6.9910^{-2}	-1.22	0.111	-1.21

Table 3. Unit square. Adapted monodomain model: convergence of the activation time ϕ_n. The error indicator e_2^n and convergence rate r_2^n being defined in (11).

n	D_n	ε_2^n: Bidomain			ε_2^n: Adapted Monodomain		
		$\chi = 1000$	$\chi = 1500$	$\chi = 2000$	$\chi = 1000$	$\chi = 1500$	$\chi = 2000$
1	177						
2	665	0.21	0.35	0.59	0.22	0.39	0.68
3	2 577	$6.3\ 10^{-2}$	$9.6\ 10^{-2}$	0.13	$6.8\ 10^{-2}$	0.10	0.13
4	10 142	$1.9\ 10^{-2}$	$3.0\ 10^{-2}$	$4.2\ 10^{-2}$	$2.1\ 10^{-2}$	$3.3\ 10^{-2}$	$4.5\ 10^{-2}$
5	40 257	$3.4\ 10^{-3}$	$6.0\ 10^{-3}$	$9.0\ 10^{-3}$	$4.4\ 10^{-3}$	$7.4\ 10^{-3}$	$1.1\ 10^{-2}$
6	160 385	$1.0\ 10^{-3}$	$1.4\ 10^{-3}$	$1.8\ 10^{-3}$	$8.3\ 10^{-4}$	$1.4\ 10^{-3}$	$2.0\ 10^{-3}$

Table 4. Unit square. Relative error estimation on ϕ_n for the bidomain and adapted monodomain models. The error indicator ε_2^n being defined in (12).

n	D_n	δ_2^n		
		$\chi = 1000$	$\chi = 1500$	$\chi = 2000$
1	177	$4.18\ 10^{-2}$	$7.07\ 10^{-2}$	0.11
2	665	$2.87\ 10^{-2}$	$3.46\ 10^{-2}$	$3.95\ 10^{-2}$
3	2 577	$2.00\ 10^{-2}$	$2.42\ 10^{-2}$	$2.73\ 10^{-2}$
4	10 142	$1.47\ 10^{-2}$	$1.76\ 10^{-2}$	$1.99\ 10^{-2}$
5	40 257	$1.12\ 10^{-2}$	$1.33\ 10^{-2}$	$1.49\ 10^{-2}$
6	160 385	$9.59\ 10^{-3}$	$1.10\ 10^{-2}$	$1.20\ 10^{-2}$

TABLE 5. Unit square. Discrepancy between the (discrete) bidomain and adapted monodomain models. The relative discrepancy δ_2^n is defined in (13).

n	D_n	Bidomain			Monodomain		
		e_2^n	r_2^n	ε_2^n	e_2^n	r_2^n	ε_2^n
1	117 285						
2	279 447	17.2		$4.3\ 10^{-2}$	18.1		$4.4\ 10^{-2}$
3	551 484	11.4	-0.60	$4.0\ 10^{-2}$	11.8	-0.63	$4.1\ 10^{-2}$
4	1 110 270	11.0	-0.05	$3.7\ 10^{-2}$	11.3	-0.06	$3.8\ 10^{-2}$

TABLE 6. 2D cut of a segmented heart. Convergence of the activation time ϕ_n for the bidomain and the monodomain models. The error indicator e_2^n and convergence rate r_2^n being defined in (11). The discretisation error estimator ε_2^n is defined in (12).

n	D_n	δ_2^n
1	117 285	$1.94\ 10^{-2}$
2	279 447	$1.65\ 10^{-2}$
3	551 484	$1.50\ 10^{-2}$
4	1 110 270	$1.35\ 10^{-2}$

TABLE 7. 2D cut of a segmented heart. Discrepancy between the (discrete) bidomain and adapted monodomain models on the heart slice geometry ($\chi = 1500$ cm^{-1}).

(Yves Bourgault) DEPARTMENT OF MATHEMATICS AND STATISTICS, UNIVERSITY OF OTTAWA.
E-mail address: ybourg@uottawa.ca

(Charles Pierre)
LABORATOIRE DE MATHÉMATIQUES ET APPLICATIONS
UNIVERSITÉ DE PAU ET DU PAYS DE L'ADOUR
AV. DE L'UNIVERSITÉ BP 1155
64013 PAU CEDEX - FRANCE
E-mail address: charles.pierre@univ-pau.fr